

Two-dimensional lattice-fluid model with water-like anomalies

C. Buzano, E. de Stefanis, A. Pelizzola, and M. Pretti

*Istituto Nazionale per la Fisica della Materia (INFM) and Dipartimento di Fisica,
Politecnico di Torino, Corso Duca degli Abruzzi 24, I-10129 Torino, Italy*

(Dated: March 22, 2022)

We investigate a lattice-fluid model defined on a two-dimensional triangular lattice, with the aim of reproducing qualitatively some anomalous properties of water. Model molecules are of the “Mercedes Benz” type, i.e., they possess a D_3 (equilateral triangle) symmetry, with three bonding arms. Bond formation depends both on orientation and local density. We work out phase diagrams, response functions, and stability limits for the liquid phase, making use of a generalized first order approximation on a triangle cluster, whose accuracy is verified, in some cases, by Monte Carlo simulations. The phase diagram displays one ordered (solid) phase which is less dense than the liquid one. At fixed pressure the liquid phase response functions show the typical anomalous behavior observed in liquid water, while, in the supercooled region, a reentrant spinodal is observed.

PACS numbers: 61.20.-p, 64.60.Cn, 64.60.My, 65.20.+w

I. INTRODUCTION

Water is an anomalous fluid with respect to several thermodynamic properties [1, 2, 3]. At ordinary pressures the solid phase (ice) is less dense than the corresponding liquid, the liquid phase has a temperature of maximum density, while both isothermal compressibility and isobaric heat capacity display a minimum as a function of temperature. Moreover, the heat capacity is unusually large. There is general agreement, among physicists, that an explanation of such anomalous properties is to be found in the peculiar features of hydrogen bonds, and the ability of water molecules to form such kind of bonds [4, 5]. It is also widely believed that the same physics should be responsible of the unusual properties of water as a solvent for apolar compounds [6, 7], that is of the hydrophobic effect, of high importance in biophysics [8]. Nevertheless, a comprehensive theory which explains all of these phenomena has not been developed yet. A lot of work has been done in “realistic” simulations [9, 10, 11, 12], based on different interaction potentials, but they generally require a large computational effort, and it is not always easy to understand which detail of the model is important to determine certain properties. On the contrary, simplified models generally need easier numerical calculations and allow quite easily to trace connections between microscopic interactions and macroscopic properties [13, 14, 15, 16, 17, 18, 19, 20, 21, 22, 23, 24]. A simplified mechanism which has been proposed to describe the relevant physics of hydrogen bonding is the following one (see for instance Refs. 5, 25). Hydrogen bond formation requires that the two involved molecules are in certain relative orientations and stay (on average) at a distance which is larger than the optimal distance for Van der Waals interaction. In other words there exists a competition between Van der Waals interaction (allowing *higher density* and *higher orientational entropy*, but resulting in a *weaker bonding*) and hydrogen bonding (requiring *lower density* and *lower orientational entropy*,

but resulting in a *stronger bonding*). This simple mechanism has been implemented in different models, both on- [22, 23, 26, 27] and off-lattice [24], in 3 [22, 23] as well as 2 dimensions [24, 26, 27]. One of them is the 2-dimensional Mercedes Benz model, originally proposed by Ben-Naim [14], in which model molecules possess three bonding arms arranged as in the Mercedes Benz logo. In recent papers by Dill and coworkers [24, 28], a similar (off-lattice) model has been simulated at constant pressure by a Monte Carlo method, allowing to describe in a qualitatively correct way several anomalous properties of liquid water and also of hydrophobic solvation. Nevertheless, in view of investigations on the behavior of water in contact with other chemical species, as it happens for instance in several biological processes, it would be desirable to obtain an even simpler representation of the physics of hydrogen bonding.

In this paper we investigate a model of the Mercedes Benz type on the triangular lattice, with a twofold purpose. As mentioned above, we are first meant to explore the possibility of obtaining a simpler model with the same underlying physical mechanism, and with qualitatively the same macroscopic properties. Moreover, we are interested in extending the model analysis to the global phase diagram and in particular to the supercooled regime, in which water anomalies are thought to find an explanation. Such a detailed analysis is just made easier by increased simplicity. Working on a lattice, we have to resort to a trick to describe hydrogen bond weakening, when the two participating molecules are too close to each other. Such a trick is similar to the one proposed by Roberts and Debenedetti for their 3-dimensional model [23, 29]. The energy of any formed bond is increased (weakened bond) of some fraction by the presence of a third molecule on a site close to the bond (i.e., on the third site of the triangle). Due to the presence of only three bonding arms, it is not possible to distinguish between hydrogen bond donors and acceptors, but this seems to be of minor importance to the physics of hydrogen bonding [24]. Let us notice that the model has the same bonding proper-

ties as the early model proposed by Bell and Lavis [13], and the same weakening criterion as the model recently investigated by Patrykiewicz and coworkers [26, 27], but here non-bonding orientations are added. Such a feature is essential to describe directional selectivity of hydrogen bonds.

The paper is organized as follows. In Sec. II we define the model in detail and analyze its ground state. In Sec. III we introduce the first order approximation in a cluster variational formulation, which we employ for the analysis. Sec. IV describes the results and Sec. V is devoted to some concluding remarks.

II. MODEL FORMULATION AND GROUND STATE

The model is defined on a two dimensional triangular lattice. A lattice site can be empty or occupied by a molecule with three equivalent bonding arms separated by $2\pi/3$ angles. Two nearest-neighbor molecules interact with an attractive energy $-\epsilon$ ($\epsilon > 0$) representing Van der Waals forces. Moreover, if two arms are pointing to each other, an orientational term $-\eta$ ($\eta > 0$) is added to mimic the formation of a hydrogen (H) bond. Due to the lattice symmetry, a particle can form three bonds at most and there are only 2 bonding orientations, when the arms are aligned with the lattice, while we assume that w non-bonding configurations exist (w is another input parameter of the model). Finally, the H bond energy is weakened by a term $cn/2$ ($c \in [0, 1]$) when a third molecule is on a site near a formed bond. In the two dimensional triangular lattice there are two such weakening sites per bond, so that a fully weakened H bond energy turns out to be $-(1-c)\eta$. Let us notice that, in the above description, H bonding is a 3-body interaction. The hamiltonian of the system can be written as a sum over the triangles

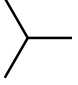
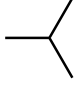
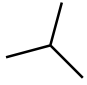
$$\mathcal{H} = \frac{1}{2} \sum_{\langle r, r', r'' \rangle} \mathcal{H}_{i_r i_{r'} i_{r''}}, \quad (1)$$

where \mathcal{H}_{ijk} is a contribution which will be referred to as triangle hamiltonian, and $i_r, i_{r'}, i_{r''}$ label site configurations for the 3 vertices r, r', r'' , respectively. Possible configurations are empty site ($i = 0$), site with a molecule in one of the 2 bonding orientations ($i = 1, 2$) or in one of the w non-bonding ones ($i = 3$) (see Tab. I). The triangle hamiltonian reads

$$\begin{aligned} \mathcal{H}_{ijk} = & -\epsilon(n_i n_j + n_j n_k + n_k n_i) \\ & -\eta[h_{ij}(1 - cn_k) + h_{jk}(1 - cn_i) + h_{ki}(1 - cn_j)], \end{aligned} \quad (2)$$

where n_i is an occupation variable, defined as $n_i = 0$ for $i = 0$ (empty site) and $n_i = 1$ otherwise (occupied site), while $h_{ij} = 1$ if the pair configuration (i, j) forms a H bond, and $h_{ij} = 0$ otherwise. Let us notice that triangle vertices are set on three triangular sublattices,

TABLE I: Possible site configurations, with corresponding labels (i) and multiplicities (w_i).

config.	empty			
i	0	1	2	3
w_i	1	1	1	w

say A, B, C , and i, j, k are assumed to denote configurations of sites placed on A, B, C sublattices respectively. Assuming also that A, B, C are ordered counterclockwise on up-pointing triangles (and then clockwise on down-pointing triangles), we can define $h_{ij} = 1$ if $i = 1$ and $j = 2$ and $h_{ij} = 0$ otherwise. Let us notice that both Van der Waals ($-\epsilon n_i n_j$) and H bond energies ($-\eta h_{ij}$), that are 2-body terms, are split between two triangles, whence the $1/2$ prefactor in Eq. (1). On the contrary the 3-body weakening terms ($\eta h_{ij} c n_k / 2$) are associated each one to a given triangle, and the $1/2$ factor is absorbed in the prefactor. Let us denote the triangle configuration probability by p_{ijk} , and assume that the probability distribution is equal for every triangle (no distinction between up- or down-pointing triangles). Taking into account that there are 2 triangles per site, we can write the following expression for the internal energy per site of an infinite lattice

$$u = \sum_{i=0}^3 \sum_{j=0}^3 \sum_{k=0}^3 w_i w_j w_k p_{ijk} \mathcal{H}_{ijk}, \quad (3)$$

The multiplicity for the triangle configuration (i, j, k) is given by $w_i w_j w_k$, where $w_i = w$ for $i = 3$ (non-bonding configuration) and $w_i = 1$ otherwise (bonding configuration or vacancy).

Let us now have a look at the ground state properties of the model. In order to do so, let us investigate the zero temperature grand-canonical free energy $\omega^\circ = u - \mu\rho$ (μ being the chemical potential and ρ the density, i.e., the average site occupation probability), which can be formally written in the same way as the internal energy u of Eq. (3), by replacing the triangle hamiltonian \mathcal{H}_{ijk} by

$$\tilde{\mathcal{H}}_{ijk} = \mathcal{H}_{ijk} - \mu \frac{n_i + n_j + n_k}{3}. \quad (4)$$

We find an infinitely dilute “gas” phase (G) with zero density and zero free energy, and an ordered “open ice” phase (I_o) with maximum number of H bonds per molecule. The latter configuration is realized through the formation of an open (honeycomb) H bond network with density $2/3$ and free energy

$$\omega_{I_o}^\circ = -\epsilon - \eta - 2\mu/3. \quad (5)$$

Another possibility is the “closed ice” phase (I_c), in which all interstitial sites are occupied and all hydrogen bonds

are fully weakened. The resulting free energy is

$$\omega_{I_c}^\circ = -3\epsilon - \eta(1 - c) - \mu. \quad (6)$$

Let us notice that it is never possible to form 3 bonds in a triangle, which means that we have frustration. It is easy to show that the G phase is stable ($\omega_{I_o}^\circ > 0$) for $\mu < \mu_{G-I_o}$, where

$$\mu_{G-I_o} = -3(\epsilon + \eta)/2, \quad (7)$$

the I_o phase is stable ($\omega_{I_o}^\circ < 0$ and $\omega_{I_o}^\circ < \omega_{I_c}^\circ$) for $\mu_{G-I_o} < \mu < \mu_{I_o-I_c}$, where

$$\mu_{I_o-I_c} = -6\epsilon + 3c\eta, \quad (8)$$

and the I_c phase is stable ($\omega_{I_c}^\circ < 0$ and $\omega_{I_c}^\circ < \omega_{I_o}^\circ$) for $\mu > \mu_{I_o-I_c}$. The I_o phase has actually a stability region, i.e., $\mu_{G-I_o} < \mu_{I_o-I_c}$, provided

$$\eta > \frac{3}{2c+1}\epsilon, \quad (9)$$

which, in the worst case ($c = 0$), reads $\eta > 3\epsilon$. We shall always work in the latter regime, which is the most significant one to describe real water properties. It is also possible to show that, at the transition point between the open and closed ice phases ($\mu = \mu_{I_o-I_c}$), any configuration built up of a honeycomb H bond network with any number of occupied interstitial sites has the same free energy. Hence we expect that the $I_o - I_c$ transition does not exist at finite temperature, and actually we shall observe a unique ice (I) phase, in which the interstitial site occupation probability gradually increases upon increasing the chemical potential.

Let us finally notice that another possible phase is a homogeneous and isotropic one in which the lattice is fully occupied and molecules can assume only bonding configurations ($i = 1, 2$). This “bonded liquid” phase, whose free energy coincides with that of the I_c phase in Eq. (6), is observed in the $w = 0$ case, studied by Patrykiewicz and others [26, 27]. In this scenario, non-bonding configurations are absent and the bonded liquid ground state has, for $c \neq 1$, the same degeneracy as the Ising triangular antiferromagnet [27]. Nevertheless, in this work we shall deal with the case $w \gg 1$, which is relevant to describe H bond directionality. In this case the closed ice phase is entropically favored with respect to the bonded liquid phase, which cannot appear at finite temperature. In conclusion, because of the introduction of non-bonding configurations, the ground state degeneracy is removed at $T = 0^+$, where only an infinitely dilute (gas) phase and a symmetry-broken (ice) phase are present. Such a phase behavior is closer to the one of water than the one obtained for $w = 0$.

III. FIRST ORDER APPROXIMATION

We shall carry out the finite temperature analysis of the model mainly by means of a generalized first order

approximation on a triangle cluster, which we introduce in the framework of the cluster variation method. The cluster variation method is an improved mean-field theory based on an approximate expression for the entropy. In Kikuchi’s original formulation [30] the entropy is obtained by an approximate counting of the number of microstates. In a modern formulation [31] the approximate entropy can be viewed as a truncation of a cluster cumulant expansion. The truncation is justified by the expected rapid vanishing of the cumulants upon increasing the cluster size, namely when the cluster size becomes larger than the correlation length of the system (the method necessarily fails near critical points) [32]. The approximation is completely defined by the maximum clusters left in the truncated expansion, usually denoted as basic clusters. One obtains a free energy functional in the cluster probability distributions, to be minimized, according to the variational principle of statistical mechanics.

For our model we choose up-pointing triangles as basic clusters (an analogous treatment works for down-pointing triangles). This approximation, which seems to be good in particular for frustrated models [33, 34], is easily shown to be equivalent to a first order approximation on a triangle cluster [13]. Let us notice that the internal energy is treated exactly, because the range of interactions does not exceed the basic cluster size, unlike the ordinary mean-field approximation. The grand-canonical free energy per site $\omega = u - \mu\rho - Ts$ (s being the entropy per site), can be written as a functional in the triangle probability distribution as

$$\beta\omega = \sum_{i=0}^3 \sum_{j=0}^3 \sum_{k=0}^3 w_i w_j w_k p_{ijk} \times \left[\beta\tilde{\mathcal{H}}_{ijk} + \ln p_{ijk} - \frac{2}{3} \ln (p_i^A p_j^B p_k^C) \right], \quad (10)$$

where $\beta \equiv 1/T$ (temperature is expressed in energy units, whence entropy in natural units) and p_i^X is the probability of the i configuration for a site on the X sublattice ($X = A, B, C$). The latter can be obtained as a marginal of the triangle configuration probability p_{ijk} , namely

$$\begin{aligned} p_i^A &= \sum_{j=0}^3 \sum_{k=0}^3 w_j w_k p_{ijk} \\ p_j^B &= \sum_{i=0}^3 \sum_{k=0}^3 w_i w_k p_{ijk} \\ p_k^C &= \sum_{i=0}^3 \sum_{j=0}^3 w_i w_j p_{ijk}. \end{aligned} \quad (11)$$

The above expressions show that the only variational parameter in ω is the triangle probability distribution, that is the 64 variables $\{p_{ijk}\}$.

The minimization of ω with respect to these variables,

with the normalization constraint

$$\sum_{i=0}^3 \sum_{j=0}^3 \sum_{k=0}^3 w_i w_j w_k p_{ijk} = 1, \quad (12)$$

can be performed by the Lagrange multiplier method, yielding the equations

$$p_{ijk} = \xi^{-1} e^{-\beta \tilde{\mathcal{H}}_{ijk}} (p_i^A p_j^B p_k^C)^{2/3}, \quad (13)$$

where ξ , related to the Lagrange multiplier, is obtained by imposing the constraint Eq. (12):

$$\xi = \sum_{i=0}^3 \sum_{j=0}^3 \sum_{k=0}^3 w_i w_j w_k e^{-\beta \tilde{\mathcal{H}}_{ijk}} (p_i^A p_j^B p_k^C)^{2/3}. \quad (14)$$

Eq. (13) is in a fixed point form, and can be solved numerically by simple iteration (natural iteration method [35]). In our case the numerical procedure can be proved to lower the free energy at each iteration [34, 35], and therefore to converge to local minima. The solution of Eq. (13) gives the equilibrium $\{p_{ijk}\}$ values, from which one can compute the thermal average of every observable. Inserting these values into Eqs. (3) and (10) gives respectively the equilibrium internal energy and free energy. The latter can be also easily expressed through the normalization constant as

$$\beta\omega = -\ln \xi, \quad (15)$$

whence ξ can be viewed as the approximate (single site) grand-canonical partition function. It is also worth mentioning that Eq. (13) preserves homogeneity ($p_i^X = p_i^Y$; $\forall i, X, Y$), due to the invariance of $\tilde{\mathcal{H}}_{ijk}$ under cycle permutation of the subscripts (see Eqs. (3) and (4)). Let us finally notice that the free energy expression Eq. (10) can be also derived by considering the model on a triangular Husimi tree (triangle cactus) [34] as a bulk free energy density, that is the free energy contribution far enough from the boundary, where an invariance condition for the configuration probability of the triangles is assumed to hold.

IV. RESULTS

A. Phase diagrams

In order to provide a first insight into the model, let us report in Fig. 1 the phase diagram in the chemical potential-temperature plane, for $\eta/\epsilon = 4$, $c = 0.5$, and $w = 50$. Three phases can be observed: An ice (I) phase, with broken symmetry among the three sublattices, a liquid (L) phase and a gas (G) phase. The latter two phases preserve the sublattice symmetry but the liquid phase has a higher density. The ice phase has a lower density than the liquid phase, and its structure reminds that of ground state ice, with interstitial sites occupied by

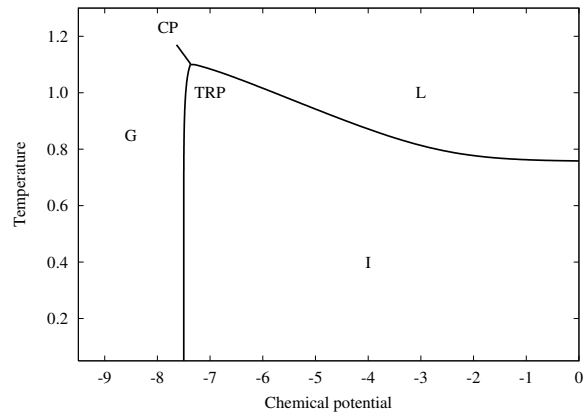


FIG. 1: Temperature (T/ϵ) vs. chemical potential (μ/ϵ) phase diagram for $w = 50$, $\eta/\epsilon = 4$, $c = 0.5$. G, L, and I denote the gas, liquid and solid (ice) phases respectively. CP denotes the critical point and TRP the triple point.

molecules in non-bonding configurations. We can observe a triple point (TRP), in which the three phases coexist, and a gas-liquid critical point (CP). All displayed transition lines are first-order. The above phase diagram shares several properties with the one of real water. Other crystalline phases, such as a real close-packed ice, cannot be reproduced by the model.

Let us now investigate the role of model parameters, by analyzing phase diagrams obtained for different values. In Fig. 2a, η/ϵ and c are left unchanged, while the number of non-bonding configurations w is varied within the interval $[20, 100]$. Upon increasing w , the liquid phase turns out to be more stable with respect to the ice phase, and the I-L transition temperature decreases. On the contrary, for lower w values, the I phase is increasingly stabilized and the I-L transition temperature increases. For $w = 20$ the whole L-G coexistence and also the critical point disappears. Such a behavior can be explained by the fact that the L phase is characterized by a higher number of non-bonding molecules than the I phase, in which bonding molecules tend to form an ordered structure. Therefore high w values largely increase the liquid phase entropy.

In Fig. 2b, w and c are held fixed and the ratio η/ϵ is varied within the interval $[3, 5]$. Let us notice that we have restricted the investigation to cases in which the orientational (H bond) interaction is stronger than the non-orientational one, which is the case for real water. It turns out that the ratio η/ϵ affects the stability of the I phase with respect to both the G and L phases. In fact higher values of η means stronger H bond, which favors the I phase, that is the only extensively H-bonded phase. On the contrary the L and G phases are dominated by non-oriented interactions with coupling constants ϵ , therefore both these two phases are unfavored by high η/ϵ values. Even in this case the L-G coexistence may become metastable.

The ice phase at high pressures has maximum density

and number of weakening molecules per H bond. Raising c , the stability of this configuration is lowered with respect to the liquid phase with few H bonds. This is shown in Fig. 2c where η/ϵ and w are fixed and the weakening parameter c is varied in its interval of definition $[0, 1]$. This trend is reversed for low w values ($w = 0$ as well), because in the latter case the liquid has the maximum number of fully weakened bonds.

In the next part of this work we focus on a particular choice of parameters ($w = 20$, $\eta/\epsilon = 3$ and $c = 0.8$) which, from the above analysis, turn out to correspond to a water-like phase diagram. Fig. 3 shows the temperature-pressure phase diagram, and Fig. 4 the temperature-density phase diagram. Let us notice that pressure P is simply given by $P = -\omega$ (the volume per site is assumed to be equal to 1, i.e., pressure is expressed in energy units), due to the fact that the free energy has been defined as a grand-canonical potential.

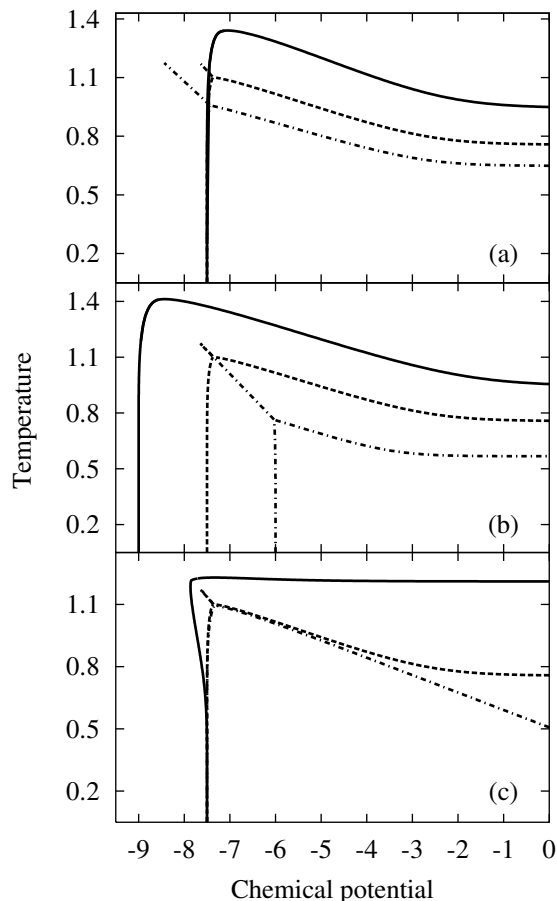


FIG. 2: The same phase diagram as in Fig. 1 (dashed lines) compared to different parameter choices: (a) $w = 20$ (solid lines) and $w = 100$ (dash-dotted lines); (b) $\eta/\epsilon = 5$ (solid lines) and $\eta/\epsilon = 3$ (dash-dotted lines); (c) $c = 0.8$ (solid lines) and $c = 0.2$ (dash-dotted lines).

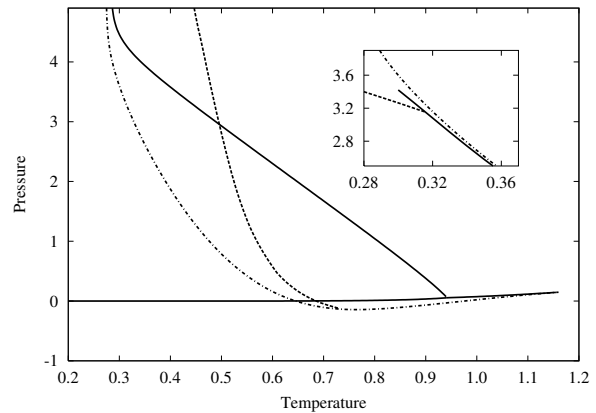


FIG. 3: Pressure (P/ϵ) vs. temperature (T/ϵ) phase diagram for $w = 20$, $\eta/\epsilon = 3$ and $c = 0.8$. Solid lines denote first order transitions, a dashed line denotes the TMD locus, and a dash-dotted line denotes the stability limit for the liquid phase. The inset displays, in addition, the locus of divergence of the density response functions at low temperature (solid line) with its “critical” point and the Kauzmann line (dashed line).

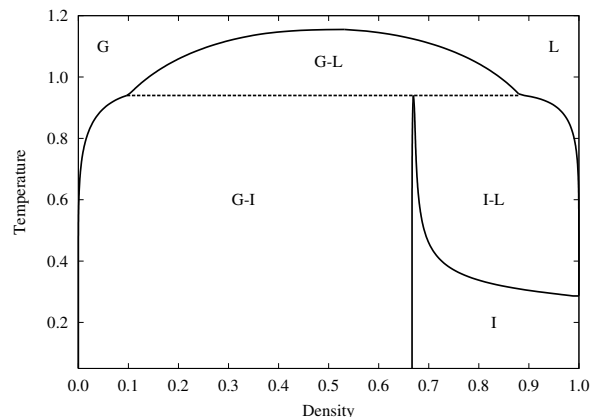


FIG. 4: Temperature (T/ϵ) vs. density (ρ) phase diagram for $w = 20$, $\eta/\epsilon = 3$ and $c = 0.8$. Solid lines denote phase boundaries; a thin dashed line corresponds to the triple point. Phase labels as in Fig. 1; double labels denote two-phase coexistence regions.

B. TMD locus and stability limits

One of the water anomalies that the present model is able to reproduce is the temperature of maximum density (TMD) along isobars for the liquid phase. Joining TMD at different pressures defines the so called TMD locus, which is a negatively sloped line in the T - P phase diagram of real water. We determine the TMD locus numerically, by adjusting the chemical potential in order to fix the pressure and then imposing that the (isobaric) thermal expansion coefficient vanishes.

The limit of stability of the liquid phase (spinodal) is the locus in which the metastable liquid ceases to be a

minimum of the free energy, and becomes a saddle point. The stability limit can be obtained by studying the eigenvalues of the hessian matrix of the free energy [36]

$$\frac{\partial^2(\beta\omega)}{\partial p_{ijk}\partial p_{i'j'k'}} = w_i w_j w_k \left\{ \frac{\delta_{ii'}\delta_{jj'}\delta_{kk'}}{p_{ijk}} - \frac{2}{3} \left[\frac{\delta_{ii'}w_{j'}w_{k'}}{p_i^A} + \frac{w_i\delta_{jj'}w_{k'}}{p_j^B} + \frac{w_i w_j \delta_{kk'}}{p_k^C} \right] \right\}. \quad (16)$$

Let us notice that, when the liquid phase stability is lost (some eigenvalue of the above matrix vanishes), also the corresponding fixed point of the natural iteration equations (13) becomes unstable. In order to determine the stability limit with respect to the symmetry-broken ice phase, it is sufficient to impose homogeneity during the iterative procedure, which is done by replacing Eqs. (11) with

$$p_i^A = p_i^B = p_i^C = \sum_{j=0}^3 \sum_{k=0}^3 w_j w_k \frac{p_{ijk} + p_{kij} + p_{jki}}{3}. \quad (17)$$

This trick cannot be applied when the liquid stability is lost with respect to a homogeneous phase, because the liquid fixed point of equations (13) becomes definitely unstable, due to divergence of the density response functions. In the latter case the spinodal is determined by solving the eigenvalue problem for the hessian matrix rewritten by forcing the homogeneity condition (17).

The results are shown in Fig. 3. The stability limit of the liquid with respect to the gas phase starts from the critical point and reaches a minimum in the negative pressure region. After this point the line becomes negatively sloped and joins continuously the stability limit with respect to the ordered ice phase. The TMD locus intersects the limit of stability in its minimum in the T - P plane, according to the predictions of Speedy and Debenedetti [37, 38, 39, 40, 41, 42, 43], based on thermodynamic consistency arguments. In fact the TMD locus causes the liquid limit of stability line to retrace, giving rise to a tensile strength maximum and to a continuous boundary. Let us recall that, while at the stability limit with respect to the gas phase, the density response functions diverge, this is not the case at the stability limit with respect to the ordered phase. Nevertheless we can observe that the density response functions tend to diverge also upon decreasing temperature, as observed experimentally. The locus of divergence, terminating at some kind of critical point, can be defined, in the framework of a simplified variational free energy forced to describe a homogeneous system, as an additional stability limit with respect to a low density liquid phase. Such “phase” corresponds to a saddle point of the original (not symmetrized) free energy, unstable with respect to the solid phase. As the low pressure solid phase reminds the ground state “open ice” structure, which is three-fold degenerate, the triangle probability distribution of the low density liquid phase turns out to be essentially an arithmetic average over the three ice distributions. The

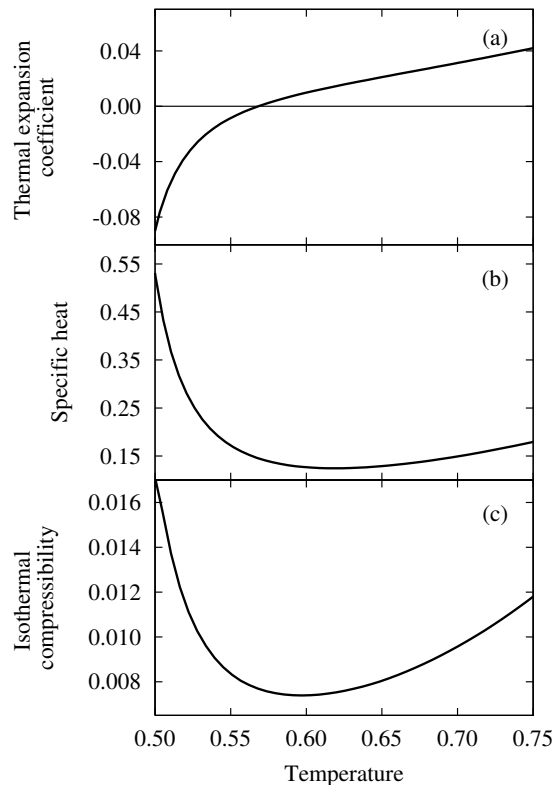


FIG. 5: Response functions at constant pressure ($P/\epsilon = 1$) as a function of temperature (T/ϵ): (a) thermal expansion coefficient ($\epsilon\alpha_P$); (b) specific heat (c_P); (c) isothermal compressibility ($\epsilon\kappa_T$).

unphysical nature of this solution is also reflected in its negative entropy. The divergence locus, together with the locus at which the liquid phase entropy vanishes (Kauzmann line), are shown for completeness in the inset of Fig. 3. Upon increasing temperature the divergence locus meets the spinodal tangentially and they become the same curve ending in the “true” gas-liquid critical point.

C. Response functions

Let us now investigate the density response functions and the specific heat of the liquid at constant pressure $P/\epsilon = 1$ (pressure is kept fixed by numerically adjusting the chemical potential μ). It turns out that these functions display an anomalous behavior similar to that of real liquid water. The first response function we consider is the thermal expansion coefficient $\alpha_P = (-\partial \ln \rho / \partial T)_P$, which is proportional to the entropy-specific volume cross-correlation. For a typical fluid α_P is always positive because if in a region of the system the specific volume is a little larger than the average, then the local entropy is also larger, i.e., the two quantities are positively correlated. On the contrary, for our model α_P (Fig. 5a) displays an anomalous behavior. As temperature is low-

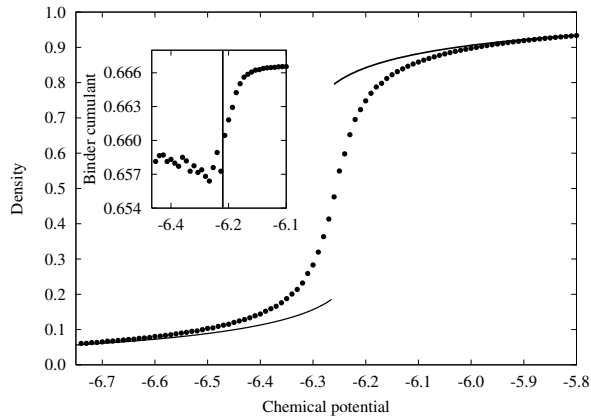


FIG. 6: Gas-liquid transition at fixed temperature ($T/\epsilon = 1.05$), upon varying the chemical potential (μ/ϵ): First order approximation results (solid line) compared to Monte Carlo simulations (scatters), for $w = 20$, $\eta/\epsilon = 3$, and $c = 0.8$. The inset displays the Binder cumulant minimum, together with the transition point predicted by the first order approximation (vertical line).

ered α_P vanishes (at the TMD), becomes negative, and finally tends to diverge. As previously mentioned, divergence can be observed only for pressure values less than some “critical” pressure. Anyway, before divergence is actually reached, the liquid loses stability with respect to the ice phase.

The trend of the isothermal compressibility $\kappa_T = (\partial \ln \rho / \partial P)_T$ is also anomalous (Fig. 5c). For a typical liquid κ_T decreases as one lowers temperature, because it is proportional to density fluctuations, which decrease upon decreasing temperature. On the contrary, in Fig. 5c we can observe that κ_T , once reached a minimum, begins to increase upon decreasing temperature. Such a behavior is observed in real liquid water. An analogous behavior characterizes the constant pressure specific heat $c_P = (-T \partial^2 \mu / \partial T^2)_P$ (Fig. 5b).

D. Numerical simulation

We have studied the model in the first order approximation to obtain easily detailed information about phase diagrams and in particular the metastable region. In order to check this approximation and obtain an estimate of its quantitative accuracy, we have also performed some (grand-canonical) Monte Carlo simulations on a 60×60 triangular lattice with periodic boundary conditions. From the very beginning, we have chosen quite a low number of non-bonding configurations for our analysis ($w = 20$), in order to increase the speed of simulation dynamics. In fact a lower w value corresponds to a smaller configuration space. We report some results in the following.

In Fig. 6 we show a first order transition between the gas and the liquid phases along a constant temperature

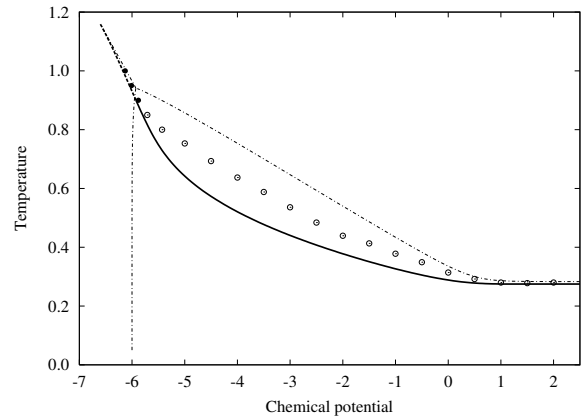


FIG. 7: Stability limits from first order approximation (thick lines) and homogeneous nucleation points from Monte Carlo simulations (scatters), for $w = 20$, $\eta/\epsilon = 3$, and $c = 0.8$. Open circles and a solid line denote the stability limit to the ice phase, filled circles and a dashed line the stability limit to the gas phase. Thin dash-dotted lines denote equilibrium phase boundaries.

path $T/\epsilon = 1.05$, quite less than the critical temperature. At the critical point the correlation length increases and the approximation may give worse predictions. Fig. 6 suggests that the first order approximation well localizes the transition and that far enough from the critical point its predictions are nearly quantitative. Of course Monte Carlo simulations display smooth density variations, due to finite size effects, but the Binder cumulant (inset), displaying a minimum, gives evidence of a first order transition.

The reentrance of the liquid stability limit, which is one of the striking features of the (metastable) phase diagram of this model, is also confirmed by simulations. Performing simulations in the metastable region, the spinodal has been determined by an arbitrary criterion for the life time of the metastable phase (100 Monte Carlo steps), as it has been done in previous studies [22]. Such a criterion allows us to find the kinetically controlled limit of supercooling (homogeneous nucleation locus), shown in Fig. 7, along with the corresponding first order approximation result. Both methods show a reentrant spinodal forming a continuous boundary. The simulations also confirm the distinction between liquid limit of stability with respect to the gas or to the ice phase, as in the first order approximation.

V. DISCUSSION AND CONCLUSIONS

In this paper we have investigated a 2-dimensional lattice model in which model molecules possess three equivalent bonding arms, and bonding energy depends on the presence of neighbor molecules, giving rise to a 3-particle interaction. The observed behavior is qualitatively similar to that of water, exhibiting the correct anomalies.

Upon supercooling, κ_T and c_P increase and α_P becomes negative and large in magnitude. Nevertheless, at ordinary pressures (less than the critical pressure) the density anomaly ($\alpha_P = 0$) is found in the metastable liquid region. We have also determined the spinodal limits to the liquid state, and pointed out the relationship between these limits and the TMD locus. The growth in the response functions upon decreasing temperature can be interpreted on the basis of a reentrant spinodal scenario. The liquid-gas spinodal meets the TMD locus at the reentrance point, as required by thermodynamic consistency. Actually the reentrant spinodal conjecture is one of the possible theoretical explanations of water anomalies, and some experimental results are consistent with this explanation [44]. Nevertheless, it is important to note that, for the specific case of water, alternative interpretations of the stability problem exist, based on the second critical point conjecture [4]. The latter, supported by molecular dynamics simulations [12], seems to be more consistent with the existence, in the negative pressure region, of a monotonic liquid-gas spinodal and a reentrant TMD locus. On the contrary, our model displays a metastable liquid state which is bounded by a spinodal both at positive as well as negative pressures, forming a continuous boundary. The lower temperature part of the boundary is the limit of stability with respect to the ordered ice phase, while the higher temperature part is the limit of stability with respect to the gas phase. While the response functions diverge at the liquid-gas spinodal, at the liquid-solid spinodal they do not, even if they tend to higher values. Anyway, in our framework, it is also possible to investigate the behavior of the unstable liquid (a saddle point of the variational free energy) and determine the locus of divergence. The latter always turns out to lie at a temperature less than the limit of stability, according to experiments [45]. It also turns out that the divergence locus terminates at some kind of critical point, meaning that response functions should not show divergent-like behavior for pressure values greater than some critical pressure.

Let us notice that a previous lattice model on the 3-

dimensional body centered cubic lattice had pointed out a qualitatively similar behavior [22]. Nevertheless, in such a model, orientational degrees of freedom of water are not treated explicitly and two equivalent sublattices are artificially distinguished by the hamiltonian. This is necessary to favor an open structured phase. Moreover, the analytical treatment is based on the determination of a temperature dependent 2-particle interaction. On the contrary in our model there exists an explicit, though simplified, modelling of hydrogen bonding and no temperature dependent interaction is introduced. The open structured phase is favored in principle by the triangular lattice structure.

We have mentioned in the Introduction that the present model is actually an extension over an early model proposed by Bell and Lavis [13] (corresponding to the case in which $w = 0$ and $c = 0$) and over a recent model investigated by Patrykiewicz and coworkers [26, 27] (corresponding to $w = 0$). The former model in the same approximation actually displays, for $\eta/\epsilon > 3$, a density anomaly (without singularities), but we have verified that the anomaly occurs in a negative entropy region. The latter model shows an unrealistic phase diagram, in which, for high enough pressure, the liquid phase extends its stability region down to zero temperature. In the present work we have shown that the addition of non-bonding configurations to such a simple class of 2-dimensional lattice models allows us to reproduce a qualitatively correct water-like behavior. Moreover, this result has been obtained in a computationally much simpler way than a conceptually similar model with continuous degrees of freedom, that is the Mercedes-Benz one. The latter model is highly appealing, because of its ability to explain most phenomena related to hydrophobicity [28]. Therefore it would be interesting to analyze also the properties of the present model for a solution of an inert (apolar) solute, whose peculiar properties are thought to be strictly related to hydrogen bonding. This goes beyond the scope of the present paper and will be the subject of a forthcoming article.

-
- [1] D. Eisenberg and W. Kauzmann, *The Structure and Properties of Water* (Oxford University Press, Oxford, 1969).
 - [2] F. Franks, ed., *Water: a Comprehensive Treatise* (Plenum Press, New York, 1982).
 - [3] H. E. Stanley et al., J. Stat. Phys. **110**, 1039 (2003).
 - [4] H. E. Stanley et al., Physica A **257**, 213 (1998).
 - [5] P. H. Poole, F. Sciortino, T. Grande, H. E. Stanley, and C. A. Angell, Phys. Rev. Lett. **73**, 1632 (1994).
 - [6] H. S. Frank and M. W. Evans, J. Chem. Phys. **13**, 507 (1945).
 - [7] F. H. Stillinger, Science **209**, 451 (1980).
 - [8] K. A. Dill, Biochemistry **29**, 7133 (1990).
 - [9] F. H. Stillinger and A. Rahman, J. Chem. Phys. **60**, 1545 (1974).
 - [10] W. L. Jorgensen et al., J. Chem. Phys. **79**, 926 (1983).
 - [11] M. W. Mahoney and W. L. Jorgensen, J. Chem. Phys. **112**, 8910 (2000).
 - [12] H. E. Stanley et al., Physica A **315**, 281 (2002).
 - [13] G. M. Bell and D. A. Lavis, J. Phys. A **3**, 568 (1970).
 - [14] A. Ben-Naim, J. Chem. Phys. **54**, 3682 (1971).
 - [15] G. M. Bell, J. Phys. C **5**, 889 (1972).
 - [16] D. A. Lavis, J. Phys. C **6**, 1530 (1973).
 - [17] G. M. Bell and D. W. Salt, J. Chem. Soc., Faraday Trans. II **72**, 76 (1976).
 - [18] D. A. Lavis and N. I. Christou, J. Phys. A **10**, 2153 (1977).
 - [19] D. A. Lavis and N. I. Christou, J. Phys. A **12**, 1869 (1979).
 - [20] P. H. E. Meijer, R. Kikuchi, and E. V. Royen, Physica A

- 115**, 124 (1982).
- [21] D. A. Huckaby and R. S. Hanna, J. Phys. A **20**, 5311 (1987).
 - [22] S. Sastry, F. Sciortino, and H. E. Stanley, J. Chem. Phys. **98**, 9863 (1993).
 - [23] C. J. Roberts and P. G. Debenedetti, J. Chem. Phys. **105**, 658 (1996).
 - [24] K. A. T. Silverstein, A. D. J. Haymet, and K. A. Dill, J. Am. Chem. Soc. **120**, 3166 (1998).
 - [25] H. E. Stanley et al., Physica A **205**, 122 (1994).
 - [26] A. Patrykiewicz, O. Pizio, and S. Sokołowski, Phys. Rev. Lett. **83**, 3442 (1999).
 - [27] P. Bruscolini, A. Pelizzola, and L. Casetti, Phys. Rev. Lett. **88**, 089601 (2002).
 - [28] K. A. T. Silverstein, A. D. J. Haymet, and K. A. Dill, J. Chem. Phys. **111**, 8000 (1999).
 - [29] C. J. Roberts, A. Z. Panagiotopoulos, and P. G. Debenedetti, Phys. Rev. Lett. **77**, 4386 (1996).
 - [30] R. Kikuchi, Phys. Rev. **81**, 988 (1951).
 - [31] G. An, J. Stat. Phys. **52**, 727 (1988).
 - [32] T. Morita, J. Math. Phys. **13**, 115 (1972).
 - [33] I. Nagahara, S. Fujiki, and S. Katsura, J. Phys. C **14**, 3781 (1981).
 - [34] M. Pretti, J. Stat. Phys. **11**, 993 (2003).
 - [35] R. Kikuchi, J. Chem. Phys. **60**, 1071 (1974).
 - [36] P. G. Debenedetti, *Metastable Liquids* (Princeton University Press, Princeton, 1996).
 - [37] R. J. Speedy, J. Phys. Chem. **86**, 982 (1982).
 - [38] R. J. Speedy, J. Phys. Chem. **86**, 3002 (1982).
 - [39] R. J. Speedy, J. Phys. Chem. **91**, 3354 (1987).
 - [40] P. Debenedetti and M. C. D'Antonio, J. Chem. Phys. **84**, 3339 (1986).
 - [41] P. Debenedetti and M. C. D'Antonio, J. Chem. Phys. **85**, 4005 (1986).
 - [42] P. Debenedetti and M. C. D'Antonio, J. Chem. Phys. **86**, 2229 (1987).
 - [43] P. Debenedetti and M. C. D'Antonio, AIChE. J. **34**, 447 (1988).
 - [44] Q. Zheng, D. J. Durben, G. H. Wolf, and C. A. Angell, Science **254**, 829 (1991).
 - [45] R. J. Speedy and C. A. Angell, J. Chem. Phys. **65**, 851 (1976).